A simulation algorithm for ultrasound liver backscattered signals

D. Zatari†, N. Botros† and F. Dunn*

† Department of Electrical Engineering, Southern Illinois University, Carbondale, Illinois 62901, USA
* Bioacoustics Research Laboratory, Department of Electrical and Computer Engineering, University of Illinois at Urbana-Champaign, Urbana, Illinois 61801, USA

Received 13 May 1995; accepted 25 August 1995

In this study, we present a simulation algorithm for the backscattered ultrasound signal from liver tissue. The algorithm simulates backscattered signals from normal liver and three different liver abnormalities. The performance of the algorithm has been tested by statistically comparing the simulated signals with corresponding signals obtained from a previous *in vivo* study. To verify that the simulated signals can be classified correctly we have applied a classification technique based on an artificial neural network. The acoustic features extracted from the spectrum over a 2.5 MHz bandwidth are the attenuation coefficient and the change of speed of sound with frequency (dispersion). Our results show that the algorithm performs satisfactorily. Further testing of the algorithm is conducted by the use of a data acquisition and analysis system designed by the authors, where several simulated signals are stored in memory chips and classified according to their abnormalities.

Keywords: ultrasound; backscattered signals; tissue; differentiation; attenuation coefficients; velocity dispersion; scatterer spacing; neural networks

Ultrasound propagation in soft tissues and its interaction with tissues are complex processes. An inherent problem is the coherent interference among wave components backscattered by different particles within the resolution cell, which causes ultrasound reflection in soft tissue to be a random process[1].

Several investigators[2–4] have reported reasonable success in characterizing disorders of liver using analytic methods such as Bayes and Nearest Neighbour statistical classifiers.

The goal of the present study is to present mathematical models of the backscattered signals for normal and three types of liver abnormalities. The study also introduces a classification technique to identify the type of abnormalities (if any). The approach taken involves analysing quantitatively the backscattered signal and applying a powerful pattern recognition technique based on a three-layer feedforward artificial neural network developed in this study. This method of interrogating the tissue is believed to be easier than visual interpretation of the time domain B-Scan image[3,4]. Accurate results may preclude the need for biopsy examination. The neural network approach has been employed by several investigators to characterize soft tissues[5–9]. It was confirmed that this approach outperforms the traditional statistical classifiers[5,8,9].

Further investigation of the algorithm performance is made when eight simulated signals are converted to real signals through hardware design. These signals are captured, digitized and stored by a data acquisition and analysis system designed and constructed by the authors.

Simulation algorithm

The propagation of the transmitted signal $x(f)$ through the tissue with power transfer function $h(f)$ can be described by the linear relation

$$r(f)=h(f)x(f) \tag{1}$$

where $r(f)$ represents the power spectrum of the received signal from a selected region of the liver specimen (see *Figure 1*). The power spectrum of $x(f)$ is often assumed Gaussian and described as[10]

$$x(f)=\frac{x_0}{\sigma\sqrt{2\pi}}\exp-\left(\frac{(f_0-f)^2}{2\sigma^2}\right) \tag{2}$$

where x_0 is the power spectrum at the centre frequency f_0 (3 MHz) and σ is a measure of the bandwidth. *Figure 2* shows the spectrum of $x(f)$.

For a resolution cell of N randomly positioned scatterers d_k, with random reflection amplitude A_k, the rf signal is the convolution of the impulse response of the transducer $x(t)$ and the tissue impulse response $h(t)$, including the effects of scattering and the absorption characteristics of the propagation path

$$r(t)=h(t)\otimes x(t) \tag{3}$$

SSDI 0041-624X(95)00059-3

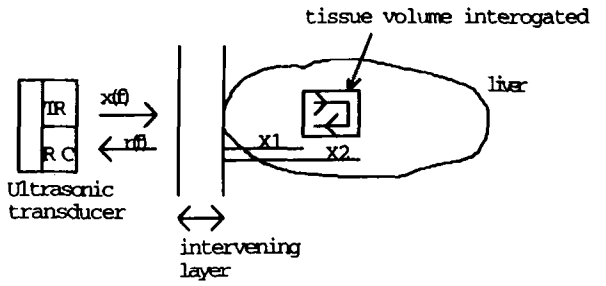

Figure 1 Pulse propagation through liver

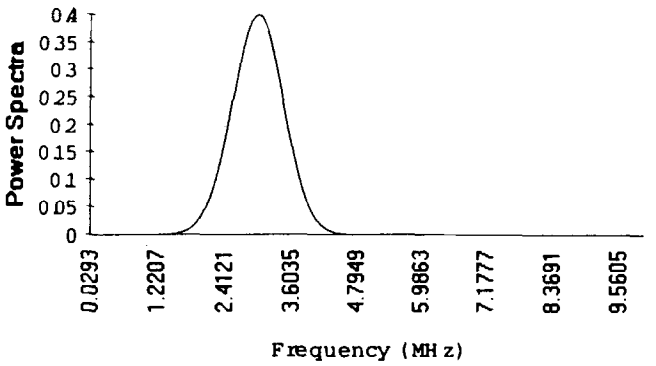

Figure 2 The power spectrum of the transmitted pulse

The tissue impulse response function is the summation of all the impulse response delta functions from all of the scatterers; that is

$$h(t)=\sum_{k=1}^{N} A_k\delta(t-\tau_k) \tag{4}$$

The summation term represents the composite nature of the backscattered echoes detected at random arrival times, τ_k, where A_k and τ_k are assumed to be uncorrelated random variables. The random arrival time is defined as $\tau_k=(2d_k/c)$ where c is the speed of sound.

Taking the Fourier transform of Equation (4), Equation (5) is obtained as

$$h(f)=\sum_{k=1}^{N} |A_k|\,e^{-j2\pi f\tau_k} \tag{5}$$

where A_k is the decaying amplitude of the echoes. The amplitude decreases with increasing depth and attenuation. This decrease is approximately exponential, $|A_k|\,e^{-2\alpha(f)d_k}$. Assuming A_k is Rayleigh distributed for large N and independent scatterer spacing, and ϕ_k is the phase that is uniformly distributed over the interval $(0, 2\pi)$, then the density function of amplitude and phase are given by[15]

$$p(A_k)=\frac{A_k}{\sigma^2}e^{-A_k/2\sigma^2} \quad \text{and} \quad p(\phi)=\frac{1}{2\pi} \quad \text{with } \phi\in(0{:}2\pi) \tag{6}$$

Empirically, the attenuation coefficient $\alpha(f)$ has been found to be expressible in terms of frequency as $\alpha(f)=a\cdot f^b$, where a and b are tissue constants[11,12]. Published values for tissue absorption constants taken from Reference 12, and for scatterer spacing taken from References 13 and 14 were employed in the simulation.

Substituting Equations (5) into Equation (1), yields the backscattered signal

$$r(f,2l)=x(f)\,e^{-2l\cdot\alpha(f)}\sum_{k=1}^{N}|A_k|\,e^{-j\omega\tau_k} \tag{7}$$

where l is tissue length. The tissue model can be described in a block diagram as shown in *Figure 3*. Equation (7) is computer simulated according to the stated assumptions, and *Figure 4* shows the power spectrum of the signal according to the equation. The simulation for A_k is made with mean $\mu=0$ and standard deviation $\sigma=1$. For better results, the amplitude is taken for every ten averaged values. The power spectra of the received signal has retained its Gaussian shape and is shifted from the centre frequency. This shift is a function of the attenuation coefficient.

Comparing the spectrum of the simulated case for a normal liver with that for an *in vivo* case, as reported previously, where these signals were measured and recorded from *in vivo* scanning of the normal liver and the same three types of abnormalities[9,17], it is evident that the simulated spectrum has retained the main features. However, through statistical analysis (total error, average, peak and standard deviation) of the power spectra of the simulated signals and the measured signals, we can see that the simulated signals are reasonably correct. We also found agreement between the characteristics of our simulated spectra and those reported by other investigators, such as Reference 13. These

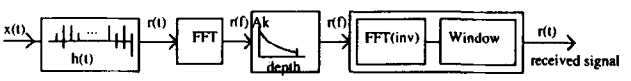

Figure 3 Block diagram of tissue model

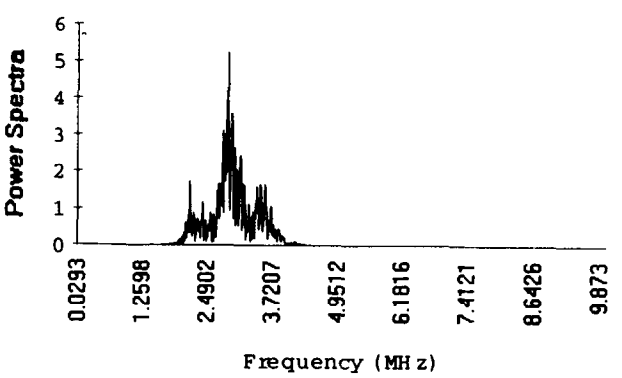

Figure 4 Power spectra of backscattered signal for normal liver

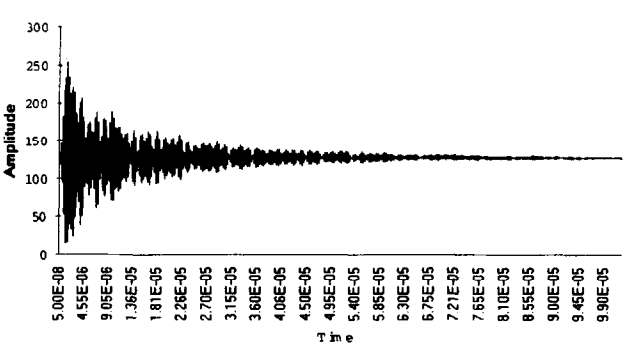

Figure 5 Simulated backscattered signal for normal liver

characteristics are mainly the Gaussian shape of the signal and the location of the peak and its shift, from centre fequency, with abnormality.

The inverse Fourier transform is applied on Equation (7) and the time domain representation of the signal is computed numerically. *Figure 5* shows the received signal as a function of time.

In the following section, a classification technique is discussed. This technique is based on extracting features from the backscattered signal, and on applying a pattern recognition algorithm to characterize the signals.

Classification technique

Feature extraction

Using Equation (7) and assuming a log spectral difference method to apply here, the attenuation coefficient in the frequency domain can be written as[9,16,17]

$$\alpha(f)=\frac{1}{2(l_2-l_1)}\cdot\ln\left(\frac{E_r(f,l_1)}{E_r(f,l_2)}\right) \quad \text{for } l_1\neq l_2 \tag{8}$$

where $E_r(f,l_1)$ and $E_r(f,l_2)$ are the power spectra of the backscattered signal from depths l_1 and l_2, respectively. Equation (8) shows that calculation of $\alpha(f)$ depends on the difference between two far-zone depths. The depth selection must satisfy the far zone criterion, and the signal must have sufficient amplitude for accurate detection of the signal.

A second feature for characterizing the tissue is the ultrasonic velocity dispersion, which can be estimated from knowledge of the attenuation coefficient as[9]

$$\delta c(\omega)=\frac{2c_0^2}{\pi}\frac{1}{2dl}\sum_{\omega_0}^{\omega}\frac{1}{\omega^2}\ln\left(\frac{E_r(f,l_1)}{E_r(f,l_2)}\right)\Delta\omega \tag{9}$$

where c_0 is the sound velocity at a convenient reference frequency ω_0, and ω is the maximum frequency encountered.

According to Equation (8), if the attenuation varies linearly with frequency, the incremental increase in speed $\delta c(\omega)$ should vary logarithmically over the defined frequency range.

A third feature is employed to improve classification results. This feature contains information about the mean scatterer spacing and the deviation from the mean. These published values represent liver classes that are similar to the classes considered in this study[13,14].

Data generation and processing

Equations (2), (6) and (7) are implemented for different liver parameters (i.e. absorption constants a and b, and scatterer spacing). The data are grouped into four liver classes such as; normal, mild liver disease, moderate/severe liver disease, and fatty liver.

Each signal is taken from depth l equal to 10 cm, and is digitized with sampling frequencey 20 MHz. It is stored in a file of length 2048 samples (i.e. 102 μs). A total of 80 files are generated (20 files per class). A window of duration 52 μs (1024 points) is applied at different positions on each signal (i.e. depth of 0, 1 and 2 cm). Consequently, three data files are generated for each case.

A fast Fourier transform (FFT) is applied to the 1024 data points, and the power spectrum is calculated. Frequencies less than 1.73 MHz, or greater than 4.2 MHz, have very small amplitudes and hence these components are filtered out. Averaging is also performed on each file and the data points per file are reduced to 33. More details of the signal processing procedure can be found in Reference 17.

The attenuation coefficient and velocity dispersion are estimated according to Equations (8) and (9). Finally, each case is represented by a file that contains two features (33 points for velocity dispersion and three points for scatterer spacing).

Pattern recognition

Pattern recognition is the process of classifying an unknown pattern and grouping it with one of the classes that represents the pattern with minimum error (or misclassification). Many researchers have employed traditional classifiers to characterize soft tissues, such as curve fitting, Bayes and Nearest Neighbour schemes. Recently, the neural network has proved to be a superior classifier[5–9], and will be pursued herein for data classification.

The input to the network is a continuous valued vector $x_1 \ldots x_{36}$. The hidden layer consists of eight nodes where the number of nodes is determined by trial and error to ensure convergence of the network. The output layer consists of four nodes, where each node represent one class (see *Figure 6*). The network is trained with an input matrix of size (36 × 40), which represents 40 vectors (ten files per class) each containing 36 data points. These vectors represent velocity dispersion as 33 points and scatterer spacing as three points.

The desired output matrix is represented by 1s and 0s. After training is completed, a data file at the input of the network can be presented for classification. Details of the network have been published elsewhere[9]. A complete algorithm is described by the flowchart given in *Figures* 7a and b.

Results

Classification results

The test set for the network consisted of 40 simulated files (ten files per class). The files used in the training (40 files, ten files per class) were not included in the test set. Data stored in these files were processed and the four simulated liver classes (normal, mild, moderate/severe, and fatty liver) were predicted by the network. These

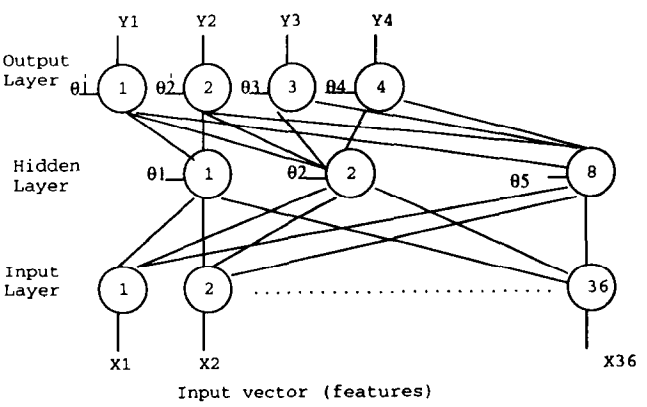

Figure 6 The artificial neural network

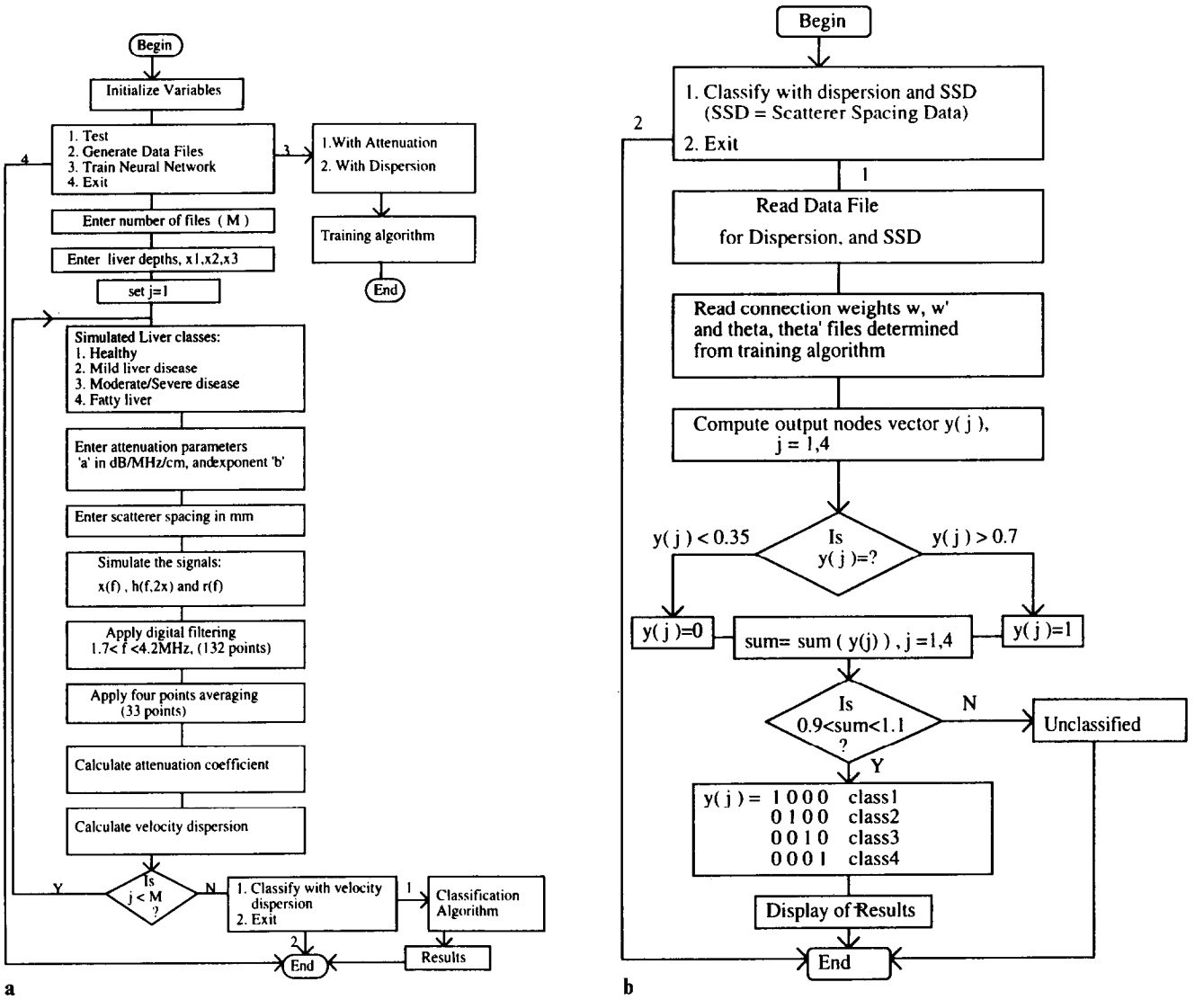

Figure 7 (a) A complete simulation algorithm. (b) Classification algorithm

classes were compared with the previously known ones. The results show that of the 40 tested cases, the system correctly classified 37 cases; all files belonging to normal liver class passed, all files belonging to class 2 passed, only 8 out of 10 files belonging to class 3 passed (the failed files were recognized as belonging to class 4), and finally 9 out of 10 files belonging to class 4 passed. When the data of the failed files were inspected, it was observed that there was severe overlap of the tissue absorption parameters. Therefore, the overall performance of the algorithm for liver classification is 92.5% for the cases examined. The validity of the simulation algorithm was further examined when an *in vivo* normal liver signal was recognized by the network as normal. *Figures 8* and *9* are examples of the variations of the attenuation coefficient and velocity dispersion, respectively, with frequency for class 1 (normal) liver specimen.

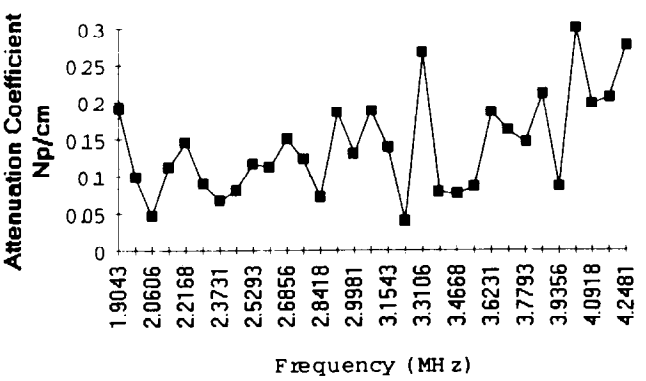

Figure 8 Attenuation coefficient for normal liver

Hardware implementation

Data acquisition system

A 20 MHz data acquisition and analysis system was designed and constructed to capture, digitize and store the signal from different depths in the liver specimen. A block diagram of the system is shown in *Figure 10*. The signal is filtered and digitized using a 10-bit analogue-to-digital converter (A/D). The digitized data are transferred to a high-speed static memory (20 ns) through a tristate data bus. The duration of each data collection (window) is 52 μs. The control unit generates

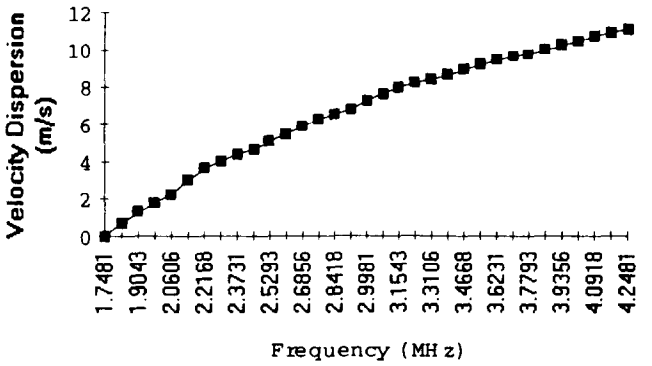

Figure 9 Velocity dispersion for normal liver

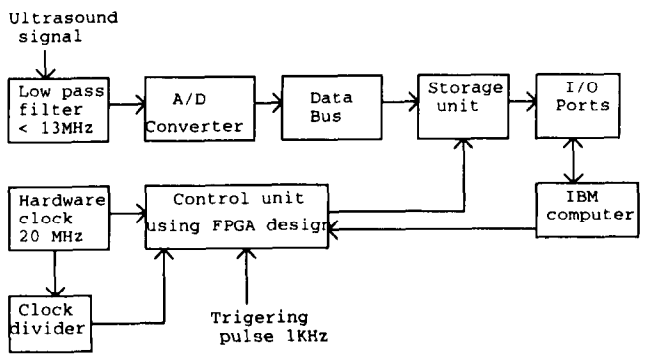

Figure 10 Block diagram of the system

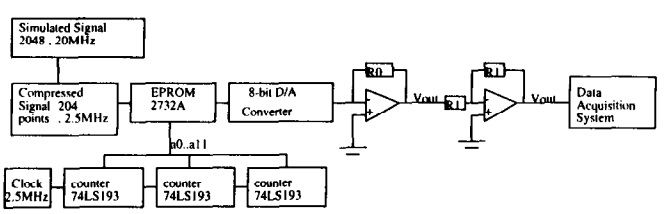

Figure 11 Construction of the simulated signal

synchronization signals during read and write cycles. It is designed and implemented using a CAD package, the field programmable gate arrays (FPGAs) technique. The control unit design is down loaded into a XILINX 3000-50 chip. The unit is triggered from a 1 kHz pulse. The depth and window are controlled using an 8-bit counter. The control unit also supplies addresses to the memories during read and write cycles. The system is completely under hardware control during the write cycle, and under software control during the read cycle. The data are accessed from the memory through communication ports. The data are stored in files for further analysis.

Hardware representation of the simulated signal

The signal was constructed with the experimental set-up shown in *Figure 11*. A window was applied on the 2048 samples of the backscattered signal for three liver depths 0, 0.5 and 1.0 cm. Three data files each of size 1024 points were formed. Each data file was then averaged and reduced to 204 points. This was due to the slow access rate of the memory (EPROM, 2.5 MHz). The 204 points were repeated up to 2048 points, in order to make the signal periodic. The file was then programmed in an EPROM chip 4k × 8 bit. The data were accessed from memory at a rate of 400 ns per sample. The digital data were converted to an analogue signal using an 8-bit digital-to-analogue converter. The analogue signal was captured and digitized by the acquisition system (50 ns per sample) and a 1k data file was produced. Each file was then averaged to 128 points (i.e. 400/50 ratio). The experiment was repeated three times per case, and a total of eight cases were investigated. A computer program written in C language was developed to perform the computation. The data files generated by the system were further analysed and processed by software as described previously. A fast Fourier transform algorithm was applied on each data file. Each file was then reduced to 64 points in the frequency domain over a bandwidth of 1.25 MHz. The attenuation coefficient and the velocity dispersion were computed for each case.

Classification results

In this case, the input to the network was a continuous valued vector $x_1 \ldots x_{19}$. An input matrix of size 19×4 was presented as a reference matrix. Four files were taken as a training set and four files as a test set. The results show that three files are differentiated correctly. The percentage of success is 75% using velocity dispersion. The field file belongs to the mild liver class, and it was recognized by the network as normal. The reason for this may be referred to the filtering and averaging of the signals.

Conclusions

The simulation algorithm presented in this study is shown to produce reasonably accurate backscattered signals for normal liver and three types of abnormalities. This success is confirmed when the authors conducted a comparison check with *in vivo* signals. It is shown that the variation with frequency of the attenuation coefficient and velocity dispersion of the generated data have approximately similar shapes when compared with *in vivo* data for normal liver, as reported earlier[9,17]. A neural network, as a pattern classifier, is employed in this study. The overall performance of the classification for the cases examined suggests that the neural network outperforms the traditional classifiers. This conclusion is supported by reports of other investigators[5–9].

In a real application, the acquisition system usually captures and digitizes the backscattered signal. However, the acquisition system is implemented in this study to capture and digitize the signals generated by the simulation algorithm.

Finally, the design of the algorithm and the system can be readily adjusted to classify among more than four liver classes.

References

1 **Ping, H.E.** Acoustic attenuation estimation for soft tissues from ultrasound echo envelope peaks *IEEE Trans Ultras Ferroelec Freq Contr* (1989) **36**

2 **Botros, N.M.** A high speed data acquisition and analysis system for ultrasonic energy measurements *IEEE Trans Instrumentation and Measurements* (1988) **37** 12–18

3 **Garra, B.S., Insana, M.F., Shawker, T.H. and Russel, M.A.** Quantitative estimation of liver attenuation and echogenicity: Normal state versus diffuse liver disease *Radiol* (1987) **162** 61–67

4 **Nicholas, D., Hill, C.R. and Nassiri, D.K.** Evaluation of backscattering coefficient for excised human tissues: principles and techniques *Ultrasound in Med & Biol* (1982) **8** 7–15

5 **Schmitz, G., Kruger, M. and Ermert, H.** Comparison of a neural network and a K-nearest neighbor classifier for the classification of different scatterer densities *Ultrasonic Imaging* (1993) **15** 168

6 **Klein Gebbinck, M.S., Verhoven, J.T.M., Thijssen, J.M. and Schouten, T.E.** Application of neural networks for the classification of diffuse liver disease by quantitative echography *Ultrasonic Imaging* (1993) **15** 168–169

7 **Hayrapetian, A.S., Chan, K.K., Weinberg, W.S. and Grant, E.G.** Neural network for ultrasound image segmentation *Ultrasonic Imaging* (1993) **15** 169

8 **DaPonte, J.S. and Sherman, P.** Classification of ultrasonic image texture by statistical discriminant analysis and neural networks *Computer Medical Imaging and Graphics* (1991) **15** 3–9

9 **Zatari, D., Botros, N. and Dunn, F.** *In vivo* liver differentiation by ultrasound using an artificial neural network *J Acoust Soc Am* (in press)

10 **Serbian, A.** Influence of attenuation upon the frequency content of the stress wave packet in graphite *J Acoust Soc Am* (1967) **42** 1052–1057

11 **Dunn, F., Edmonds, P.D. and Fry, W.J.** Absorption and dispersion of ultrasound in biological media, in *Biological Engineering* (Ed Schwan H.P.) McGraw-Hill, New York (1969) 205–332

12 **Lin, T. and Ophir, J.** Frequency-dependent ultrasonic differentiation of normal and diffusely diseased liver *J Acoust Soc Am* (1987) **82**

13 **Sommer, F.G., Linda, F.J., Carroll B.A. and Macovski, A.** Ultrasonic characterization of abdominal tissues via digital analysis of backscattered wave forms *Radiology* (1981) **141** 811–817

14 **Fellingham, L.L. and Sommer, F.G.** Ultrasonic characterization of tissue structure in the *in vivo* human liver and spleen *IEEE Trans on Sonics and Ultrasonic* (1984) **31**

15 **Li Weng et al.,** Nonuniform phase distribution in ultrasound speckle analysis—Part I: background and experimental demonstration *IEEE Trans Ultras Ferroelec Freq Contr* (1992) **39**

16 **Dines, K.A. and Kak, A.C.** Ultrasound attenuation tomography of soft tissues *Ultrason Imag* (1979) **1** 16–33

17 **Botros, N.** *In vivo* tissue differentiation through digital signal processing, PhD Dissertation, Norman Oklahoma (1984)